CHAPTER 180

Nonlinear Wave Transformation over a Submerged Triangular Breakwater

Lifen Dong[1], Akira Watanabe and Masahiko Isobe[2]

Abstract

This study deals with wave transformation over a submerged triangular breakwater that is composed of a series of elements with a triangular horizontal cross-section. The idea of such a triangular breakwater is founded on the use of the wave refraction due to peculiar spatial change in water depth around it.

A numerical model is developed to predict nonlinear wave transformation over and around the breakwater on the basis of fully nonlinear wave equations proposed by Isobe (1994). Laboratory experiment has also been conducted in a wave basin. The validity of the numerical model is examined by comparing the computations with the measurements.

1. Introduction

When waves propagate over a submerged triangular breakwater, wave refraction will happen. The superiority of a submerged triangular breakwater lies in its capability of controlling the wave direction as well as the height as compared to conventional submerged breakwaters with rectangular cross-section. For example, a breakwater as shown in Fig. 1 (a) can control even the longshore current through the change in the wave direction, whereas the one as illustrated in Fig. 1 (b) may be employed to increase the wave height in the locations where the waves converge for purposes such as effective wave energy use and surfing.

This paper presents the results of numerical computation based on fully nonlinear mild-slope equations proposed by Isobe and compares them with those of a laboratory experiment for breakwaters of the type (b).

[1]Research Engineer, River Engineering Consultants Co., Ltd., Ohyama Higashichou 40-5, Itabashi-ku, Tokyo, 113, Japan.

[2]Professor, Dept. of Civil Eng., Univ. of Tokyo, Tokyo, 113, Japan.

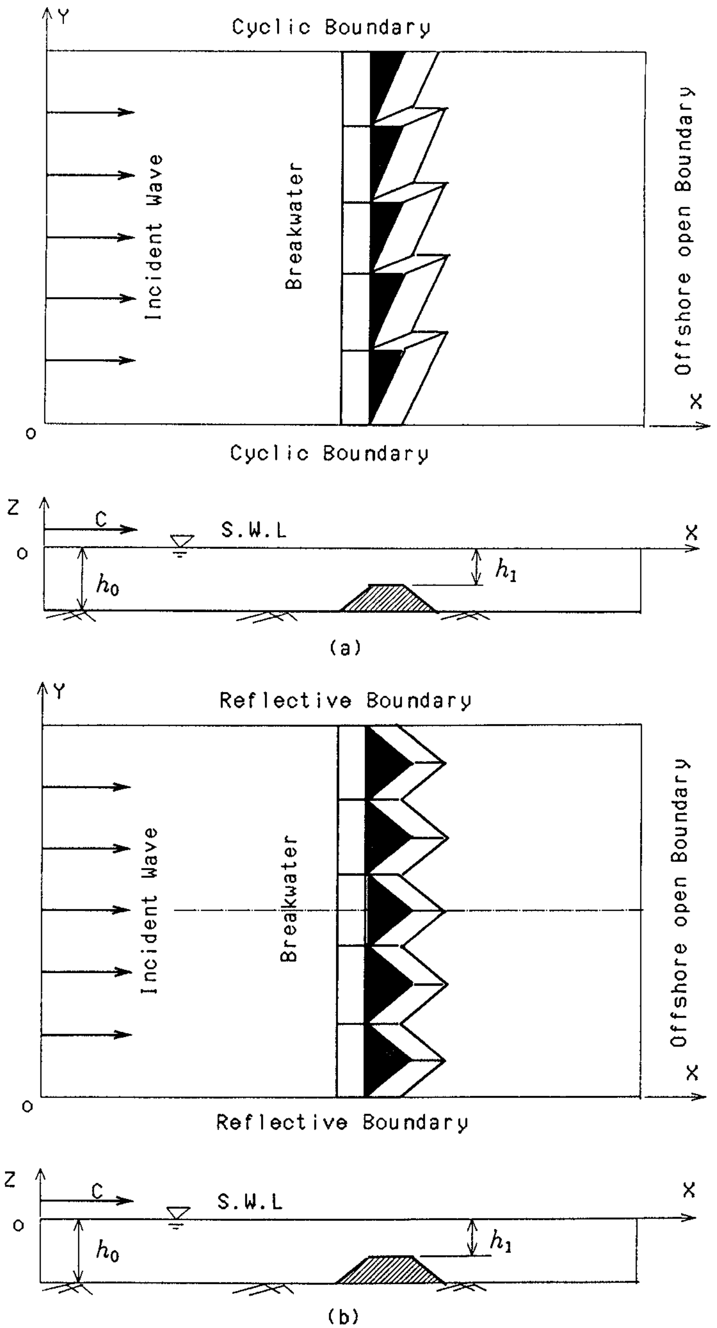

Fig. 1 Two types of submerged triangular breakwaters.

2. Numerical Model

2.1 Governing equations

The mild-slope nonlinear equations proposed by Isobe (1994) are as follows:

$$Z_\alpha^\eta \frac{\partial \eta}{\partial t} + \nabla(A_{\alpha\beta}\nabla f_\beta) - B_{\alpha\beta} f_\beta + (C_{\beta\alpha} - C_{\alpha\beta})\nabla f_\beta \nabla h + \frac{\partial Z_\beta^\eta}{\partial h} Z_\alpha^\eta f_\beta \nabla\eta\nabla h = 0 \quad (1)$$

$$g\eta + Z_\beta^\eta \frac{\partial f_\beta}{\partial t} + \frac{1}{2} Z_\gamma^\eta Z_\beta^\eta \nabla f_\gamma \nabla f_\beta + \frac{1}{2}\frac{\partial Z_\gamma^\eta}{\partial z}\frac{\partial Z_\beta^\eta}{\partial z} f_\gamma f_\beta + \frac{\partial Z_\gamma^\eta}{\partial h} Z_\beta^\eta f_\gamma \nabla f_\beta \nabla h = 0 \quad (2)$$

where $Z_\alpha^\eta = Z_\alpha|_{z=\eta}$, h is the water depth, and the water surface elevation η and the function f_α are unknown variables. The vertical distribution function Z_α is related to the velocity potential ϕ and defined as

$$\phi(x,y,z,t) = \sum_{\alpha=0}^{N} Z_\alpha(z, h(x,y)) f_\alpha(x,y,t) \quad (3)$$

$$Z_\alpha(z, h(x,y)) = \left(1 + \frac{z}{h}\right)^{2\alpha} \quad (4)$$

The coefficients $A_{\alpha\beta}$, $B_{\alpha\beta}$ and $C_{\alpha\beta}$ can be obtained from Z_α by

$$A_{\alpha\beta} = \int_{-h}^{\eta} Z_\alpha Z_\beta dz \quad (5)$$

$$B_{\alpha\beta} = \int_{-h}^{\eta} \frac{\partial Z_\alpha}{\partial z}\frac{\partial Z_\beta}{\partial z} dz \quad (6)$$

$$C_{\alpha\beta} = \int_{-h}^{\eta} \frac{\partial Z_\alpha}{\partial h} Z_\beta dz \quad (7)$$

2.2 Boundary conditions

For the present case, the following perfectly reflective boundary condition is imposed on the side boundaries by virtue of the symmetry of the structure and the resulting wave field.

$$\frac{\partial \phi}{\partial y} = 0 \quad (8)$$

By substituting the expression of ϕ into Eq. (8), the following two expressions are obtained as side boundary conditions.

$$\frac{\partial \eta}{\partial y} = 0, \qquad \frac{\partial f_\alpha}{\partial y} = 0 \quad (9)$$

The Sommerfeld radiation condition is used on the onshore open boundary.

$$\frac{\partial \phi}{\partial t} + C\frac{\partial \phi}{\partial \vec{n}} = 0 \quad (10)$$

The substitution of ϕ yields the onshore boundary conditions as follows:

$$\frac{\partial \eta}{\partial t} + C\frac{\partial \eta}{\partial \bar{n}} = 0, \qquad \frac{\partial f_\alpha}{\partial t} + C\frac{\partial f_\alpha}{\partial \bar{n}} = 0, \tag{11}$$

in which $\bar{n}$ is the length of the mean direction vector of transmitted waves and C denotes the wave celerity.

The offshore boundary condition is given by

$$\cos\bar{\alpha}_r \frac{\partial \phi}{\partial t} - C\frac{\partial \phi}{\partial x} = (1 + \cos\bar{\alpha}_r)\frac{\partial \phi_0}{\partial t} \tag{12}$$

where ϕ_0, the potential of the incident waves, is expressed as

$$\phi_0 = \sum_{\alpha=0}^{N} Z_\alpha f_{\alpha 0} = Z_\alpha f_{\alpha 0} \tag{13}$$

Substituting of the expressions of ϕ and ϕ_0 into Eq. (12), we obtain

$$\cos\bar{\alpha}_r \frac{\partial \eta}{\partial t} - C\frac{\partial \eta}{\partial x} = (1 + \cos\bar{\alpha}_r)\frac{\partial \eta_0}{\partial t} \tag{14}$$

$$\cos\bar{\alpha}_r \frac{\partial f_\alpha}{\partial t} - C\frac{\partial f_\alpha}{\partial x} = (1 + \cos\bar{\alpha}_r)\frac{\partial f_{\alpha 0}}{\partial t} \tag{15}$$

where η_0 is the water surface elevation of the incident waves and $\bar{\alpha}_r$ is the mean direction of reflected waves.

2.3 Expression of incident waves

Even in the computation of nonlinear wave transformation, the incident waves will be reasonally expressed by a small amplitude wave theory if the Ursell number is not so large at the offshore boundary. Assuming that the incident waves are monochromatic sinusoidal waves propagating along the x-direction, their potential ϕ_0 can be expressed as

$$\begin{aligned} \phi_0 &= \frac{a_0 g}{\sigma}\frac{\cosh k_0(z+h_0)}{\cosh k_0 h_0}\sin(k_0 x - \sigma t) && (16) \\ &= \sum_{\alpha=0}^{N} Z_\alpha f_{\alpha 0} && (17) \end{aligned}$$

which corresponds to the water surface displacement η_0 given by

$$\eta_0 = a_0 \cos(k_0 x - \sigma t) \tag{18}$$

where a_0 and k_0 are the amplitude and the wave number of the incident waves, h_0 is the offshore water depth, and σ is the angular frequency.

By expanding $\cosh k_0(z + h_0)$, ϕ_0 can be expressed as

$$\phi_0 = \sum_{\alpha=0}^{N} \frac{a_0 g}{\sigma} \frac{(k_0 h_0)^{2\alpha}}{(2\alpha)! \cosh k_0 h_0} \sin(k_0 x - \sigma t) \left(1 + \frac{z}{h_0}\right)^{2\alpha} \tag{19}$$

From this equation we obtain

$$f_{\alpha 0} = \frac{a_0 g}{\sigma} \frac{(k_0 h_0)^{2\alpha}}{(2\alpha)! \cosh k_0 h_0} \sin(k_0 x - \sigma t) \tag{20}$$

2.4 Finite difference equations

Numerical solutions of the governing equations are obtained using a finite difference technique. Central difference and forward difference are adopted in space and in time, respectively. To the nonlinear equations into a finite difference form for the present two-dimensional problem, ADI (Alternating Direction Implicit) scheme (Fletcher, 1987) is employed, namely, Eqs. (4.1) and (4.2) are splitted into x–sweep and y–sweep finite difference equations.

x–sweep

During the first half-step the following discretization is made.

$$\begin{aligned}
&Z_\alpha^\eta \frac{\eta_{i,j}^{m+\frac{1}{2}} - \eta_{i,j}^m}{\Delta t/2} + A_{\alpha\beta i,j} \frac{f_{\beta(i+1),j}^{m+\frac{1}{2}} + f_{\beta(i-1),j}^{m+\frac{1}{2}} - 2 f_{\beta i,j}^{m+\frac{1}{2}}}{\Delta x^2} \\
&+ A_{\alpha\beta i,j} \frac{f_{\beta i,j+1}^m + f_{\beta i,j-1}^m - 2 f_{\beta i,j}^m}{\Delta y^2} - B_{\alpha\beta} f_{\beta i,j}^{m+\frac{1}{2}} \\
&+ \frac{A_{\alpha\beta(i+1),j} - A_{\alpha\beta(i-1),j}}{2\Delta x} \frac{f_{\beta(i+1),j}^{m+\frac{1}{2}} - f_{\beta(i-1),j}^{m+\frac{1}{2}}}{2\Delta x} \\
&+ \frac{A_{\alpha\beta i,j+1} - A_{\alpha\beta i,j-1}}{2\Delta y} \frac{f_{\beta i,j+1}^m - f_{\beta i,j-1}^m}{2\Delta y} \\
&+ (C_{\beta\alpha} - C_{\alpha\beta}) \frac{f_{\beta(i+1),j}^{m+\frac{1}{2}} - f_{\beta(i-1),j}^{m+\frac{1}{2}}}{2\Delta x} \frac{h_{i+1,j} - h_{i-1,j}}{2\Delta x} \\
&+ (C_{\beta\alpha} - C_{\alpha\beta}) \frac{f_{\beta i,j+1}^m - f_{\beta i,j-1}^m}{2\Delta y} \frac{h_{i,j+1} - h_{i,j-1}}{2\Delta y} \\
&+ \frac{\partial Z_\beta^\eta}{\partial h} Z_\alpha^\eta f_{\beta i,j}^{m+\frac{1}{2}} \left(\frac{\eta_{i+1,j}^m - \eta_{i-1,j}^m}{2\Delta x} \frac{h_{i+1,j} - h_{i-1,j}}{2\Delta x} + \frac{\eta_{i,j+1}^m - \eta_{i,j-1}^m}{2\Delta y} \frac{h_{i,j+1} - h_{i,j-1}}{2\Delta y} \right) \\
&= 0
\end{aligned} \tag{21}$$

$$\begin{aligned}
&g\eta_{i,j}^{m+\frac{1}{2}} + Z_\beta^\eta \frac{f_{\beta i,j}^{m+\frac{1}{2}} - f_{\beta i,j}^m}{\Delta t/2} + \frac{1}{2} Z_\gamma^\eta Z_\beta^\eta \left(\frac{f_{\gamma(i+1),j}^m - f_{\gamma(i-1),j}^m}{2\Delta x} \frac{f_{\beta(i+1),j}^{m+\frac{1}{2}} - f_{\beta(i-1),j}^{m+\frac{1}{2}}}{2\Delta x} \right) \\
&+ \frac{1}{2} Z_\gamma^\eta Z_\beta^\eta \left(\frac{f_{\gamma i,j+1}^m - f_{\gamma i,j-1}^m}{2\Delta y} \frac{f_{\beta i,j+1}^m - f_{\beta i,j-1}^m}{2\Delta y} \right) + \frac{1}{2} \frac{\partial Z_\gamma^\eta}{\partial z} \frac{\partial Z_\beta^\eta}{\partial z} f_{\gamma i,j}^m f_{\beta i,j}^{m+\frac{1}{2}}
\end{aligned}$$

$$
+\left(\frac{f^{m+\frac{1}{2}}_{\beta(i+1),j}-f^{m+\frac{1}{2}}_{\beta(i-1),j}}{2\triangle x}\frac{h_{i+1,j}-h_{i-1,j}}{2\triangle x}+\frac{f^{m}_{\beta i,j+1}-f^{m}_{\beta i,j-1}}{2\triangle y}\frac{h_{i,j+1}-h_{i,j-1}}{2\triangle y}\right)
$$
$$
\frac{\partial Z^{\eta}_{\gamma}}{\partial h}f^{m}_{\gamma i,j}Z^{\eta}_{\beta}
$$
$$
=0 \tag{22}
$$

in which, $\triangle x$ and $\triangle y$ are the space intervals and $\triangle t$ is the time interval. The quantities $\eta^{m+\frac{1}{2}}_{i,j}$ and $f^{m+\frac{1}{2}}_{\beta i,j}$ are the unknowns, whereas $\eta^{m}_{i,j}$, $f^{m}_{\beta i,j}$ and other parameters are given in the previous time step m.

y–sweep

During the second half-step the following discretization is made.

$$
Z^{\eta}_{\alpha}\frac{\eta^{m+1}_{i,j}-\eta^{m+\frac{1}{2}}_{i,j}}{\triangle t/2}+A_{\alpha\beta i,j}\frac{f^{m+\frac{1}{2}}_{\beta(i+1),j}+f^{m+\frac{1}{2}}_{\beta(i-1),j}-2f^{m+\frac{1}{2}}_{\beta i,j}}{\triangle x^{2}}
$$
$$
+A_{\alpha\beta i,j}\frac{f^{m+1}_{\beta i,j+1}+f^{m+1}_{\beta i,j-1}-2f^{m+1}_{\beta i,j}}{\triangle y^{2}}-B_{\alpha\beta}f^{m+1}_{\beta i,j}
$$
$$
+\frac{A_{\alpha\beta(i+1),j}-A_{\alpha\beta(i-1),j}}{2\triangle x}\frac{f^{m+\frac{1}{2}}_{\beta(i+1),j}-f^{m+\frac{1}{2}}_{\beta(i-1),j}}{2\triangle x}
$$
$$
+\frac{A_{\alpha\beta i,j+1}-A_{\alpha\beta i,j-1}}{2\triangle y}\frac{f^{m+1}_{\beta i,j+1}-f^{m+1}_{\beta i,j-1}}{2\triangle y}
$$
$$
+(C_{\beta\alpha}-C_{\alpha\beta})\frac{f^{m+\frac{1}{2}}_{\beta(i+1),j}-f^{m+\frac{1}{2}}_{\beta(i-1),j}}{2\triangle x}\frac{h_{i+1,j}-h_{i-1,j}}{2\triangle x}
$$
$$
+(C_{\beta\alpha}-C_{\alpha\beta})\frac{f^{m+1}_{\beta i,j+1}-f^{m+1}_{\beta i,j-1}}{2\triangle y}\frac{h_{i,j+1}-h_{i,j-1}}{2\triangle y}
$$
$$
+\frac{\partial Z^{\eta}_{\beta}}{\partial h}Z^{\eta}_{\alpha}f^{m+1}_{\beta i,j}\left(\frac{\eta^{m+\frac{1}{2}}_{i+1,j}-\eta^{m+\frac{1}{2}}_{i-1,j}}{2\triangle x}\frac{h_{i+1,j}-h_{i-1,j}}{2\triangle x}+\frac{\eta^{m+\frac{1}{2}}_{i,j+1}-\eta^{m+\frac{1}{2}}_{i,j-1}}{2\triangle y}\frac{h_{i,j+1}-h_{i,j-1}}{2\triangle y}\right)
$$
$$
=0 \tag{23}
$$

$$
g\eta^{m+1}_{i,j}+Z^{\eta}_{\beta}\frac{f^{m+1}_{\beta i,j}-f^{m+\frac{1}{2}}_{\beta i,j}}{\triangle t}+\frac{1}{2}Z^{\eta}_{\gamma}Z^{\eta}_{\beta}\left(\frac{f^{m+\frac{1}{2}}_{\gamma(i+1),j}-f^{m+\frac{1}{2}}_{\gamma(i-1),j}}{2\triangle x}\frac{f^{m+\frac{1}{2}}_{\beta(i+1),j}-f^{m+\frac{1}{2}}_{\beta(i-1),j}}{2\triangle x}\right)
$$
$$
+\frac{1}{2}Z^{\eta}_{\gamma}Z^{\eta}_{\beta}\left(\frac{f^{m+\frac{1}{2}}_{\gamma i,j+1}-f^{m+\frac{1}{2}}_{\gamma i,j-1}}{2\triangle y}\frac{f^{m+1}_{\beta i,j+1}-f^{m+1}_{\beta i,j-1}}{2\triangle y}\right)+\frac{1}{2}\frac{\partial Z^{\eta}_{\gamma}}{\partial z}\frac{\partial Z^{\eta}_{\beta}}{\partial z}f^{m}_{\gamma i,j}f^{m+1}_{\beta i,j}
$$
$$
+\left(\frac{f^{m+\frac{1}{2}}_{\beta(i+1),j}-f^{m+\frac{1}{2}}_{\beta(i-1),j}}{2\triangle x}\frac{h_{i+1,j}-h_{i-1,j}}{2\triangle x}+\frac{f^{m+1}_{\beta i,j+1}-f^{m+1}_{\beta i,j-1}}{2\triangle y}\frac{h_{i,j+1}-h_{i,j-1}}{2\triangle y}\right)
$$

$$\frac{\partial Z_{\gamma}^{\eta}}{\partial h} f_{\gamma i,j}^{m} Z_{\beta}^{\eta} = 0 \tag{24}$$

in which $\eta_{i,j}^{m+1}$, $f_{\beta i,j}^{m+1}$ are the unknowns, and $\eta_{i,j}^{m+\frac{1}{2}}$, $f_{\beta i,j}^{m+\frac{1}{2}}$ and other parameters are given at the previous time step $(m + \frac{1}{2})$.

2.5 Numerical solutions

Solutions of the finite difference equations are obtained by using the boundary conditions given above. In the numerical computation, the intervals of space and time are taken as follows: $\Delta x < L_0/20$, $\Delta y < L_0/20$, $\Delta t = T/250$, where, T is the wave period and L_0 is the wavelength.

At any time step m, the water surface elevation $\eta_m(x_i, y_j)$ can be obtained by solving the above equations. Then the root mean square value of the water surface displacement $\eta_{\mathrm{rms}}(x_i, y_j)$ can be given by

$$\eta_{\mathrm{rms}}(x_i, y_j) = \sqrt{\sum_{m=1}^{n} \eta_m^2(x_i, y_j)/n} \tag{25}$$

where n is the total sampling number of water surface elevation within several wave periods.

3. Laboratory Experiment

3.1 Experimental setup

In order to observe the wave deformation process and to examine the numerical computation model, a two-dimensional laboratory experiment on wave transformation over submerged triangular breakwaters has been made in a wave basin, of which the flow domain is 3.55×0.75 m. A flap-type wave maker is equiped to generate regular waves, and a wave absorber is placed on the onshore boundary in order to avoid the wave reflectoin.

Only a half element of the breakwater has been taken in the experiment (as well as in the computation) because of the symmetry of the breakwater as shown in Fig. 1 (b). Two types of model breakwaters have been modeled. The first one has a purely triangular horizontal cross-section with seaward and shoreward side slope of 1/3, whereas the second one has a cross-section composed of triangular and rectangular parts as shown in Fig. 2. In all the cases, the direction of incident waves is in parallel to the x-axis and no wave breaking over the breakwater has occurred.

3.2 Data acquisition and processing

The water surface displacement was measured at many points with small spacing in the x-direction along the nine sections shown in Fig. 2 with the capacitance-

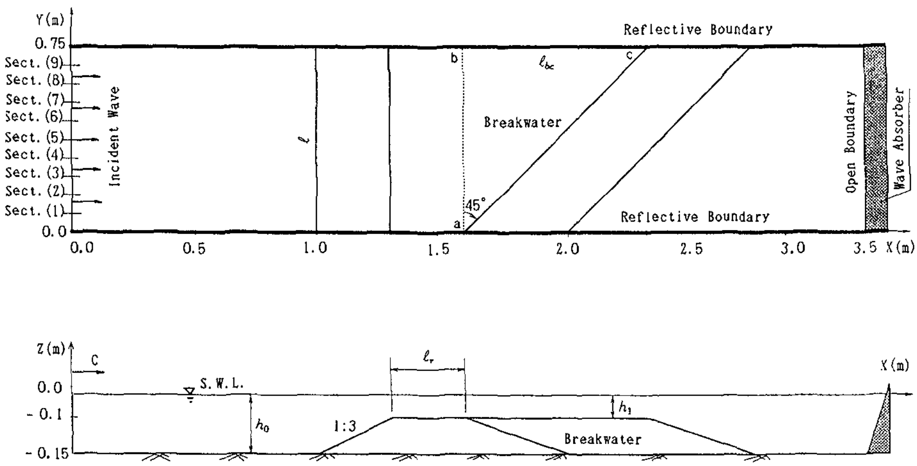

Fig. 2 Experimental setup.

type wave gages. After preliminary processing, the root mean square value of the water surface elevation $\eta_{\rm rms}$ was obtained for every point.

$$\eta_{\rm rms} = \sqrt{\sum_{i=1}^{n} \eta^2(t_i)/n} \tag{26}$$

By utilizing the separation technique for incident and reflected wave components (Goda and Suzuki,1976) from two adjacent wave records measured along the x-direction at the same time, the amplitude of incident waves a_{0j} was evaluated. Then the root mean square of water surface displacement of the incident waves was obtained by using the following expression.

$$\eta_{0\rm rms} = \sqrt{\sum_{j=1}^{m} \frac{a_{0j}^2}{2}} \tag{27}$$

where m is the number of incident wave components.

Finally relative values of the water surface elevation $\eta_{\rm rms}/\eta_{0\rm rms}$ were calculated.

4. Results and Conclusions

4.1 Results

For the two types of breakwaters, the experiment and computation were carried out under various incident wave conditions. In the numerical computation, the mean direction angle of reflected waves $\bar{\alpha}_r$ was taken as 0.0 degree for all the cases, and the mean direction of transmitted waves was assumed to be parallel to the x-direction at any grid point on the onshore boundary. The range of α in the vertical distribution function $Z_\alpha(z)$ is taken from 0 to 3, i.e., four terms are taken in the expression of velovity potential ϕ.

Fig. 3 shows examples of the comparisions between the measurements and the computations of the relative root mean square of the water surface displacement along the sections (1), (3), (5), (7) and (9) for the first type of the breakwater. The total water depth is 15 cm, the breakwater height is 10 cm, and the incident wave height and period are 0.85 cm and 1.0 s. Fig. 4 shows the comparisions between the measurements and the computations of time histories of the water surface displacements at several points along the x-direction for the same condition. Both the figures demonstrate a rather good agreement between the measurements and the computations.

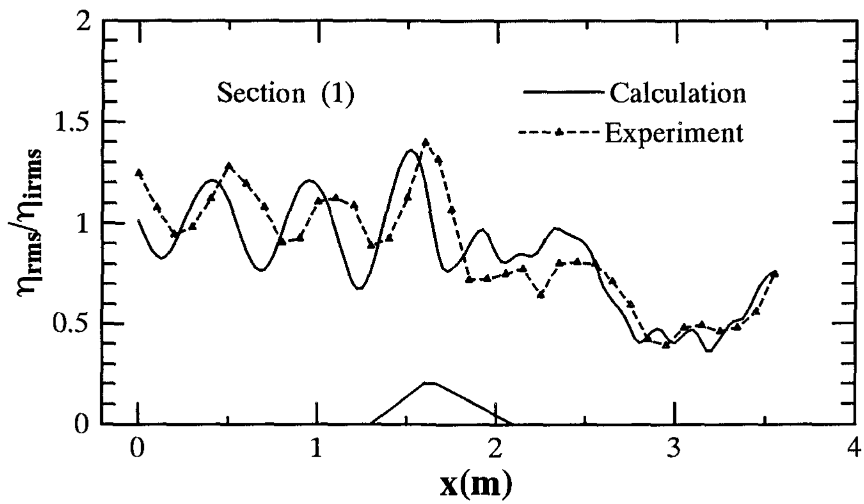

Fig. 3.1 Distributions of RMS of surface displacements.

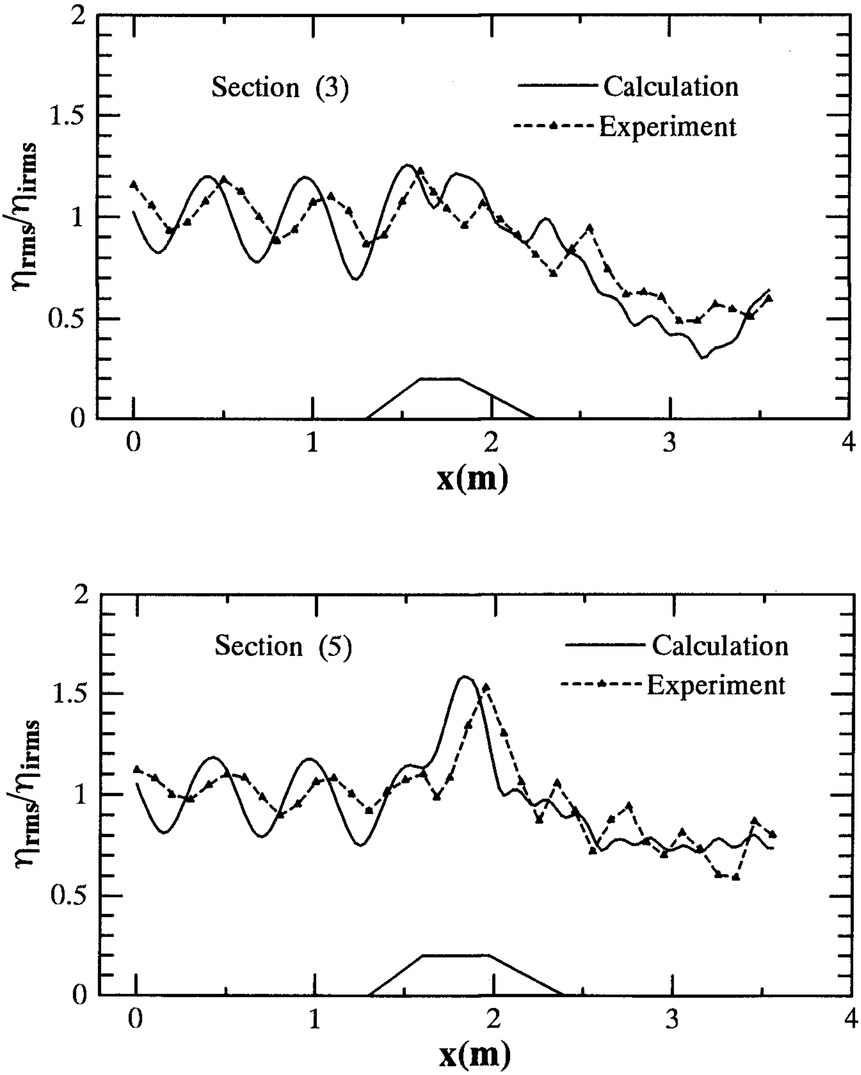

Fig. 3.2 Distributions of RMS of surface displacements.

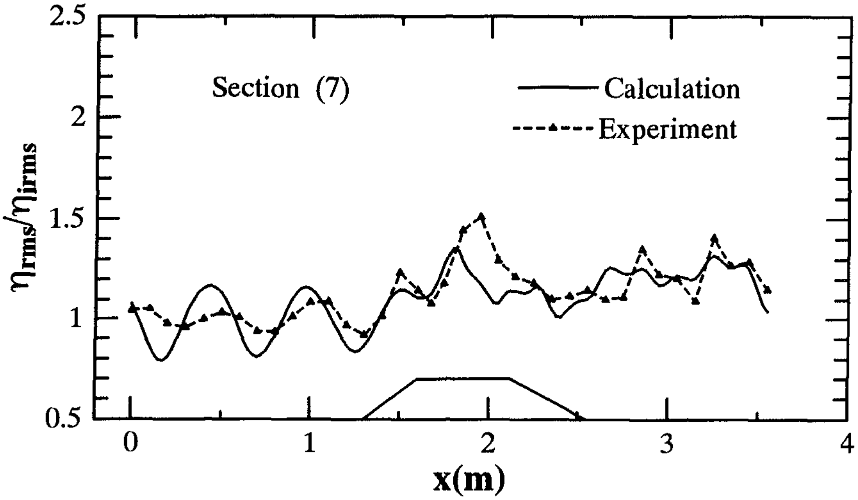

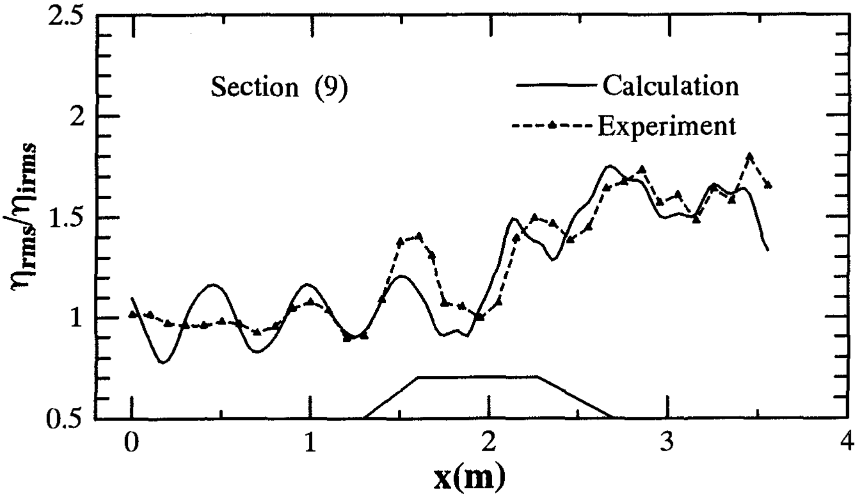

Fig. 3.3 Distributions of RMS of surface displacements.

In Fig. 3, we can see significant variations in the cross-shore distributions of water surface displacements for different sections. Usually the water surface displacement in the region behind the breakwater increases from section (1) to section (9); the mean relative water surface elevations are less than unity from sections (1) to (7), while they are larger than unity for the section (9). The mean value of the transmission coefficients reaches a value of 0.85.

In Fig. 4, a remarkable change in the time histories of the water surface displacements along the x-direction can be seen. In the region before the breakwater, the water surface elevation at position 1 (x =0.5 m) behaves without peculiarities, whereas the time history at position 4 (x =2.0 m) on the top of the breakwater shows strongly nonlinearity with steep peaks. In the region behind the breakwater, two peaks appear in the wave profiles at position 5 (x =2.5 m), i.e., higher harmonics exist.

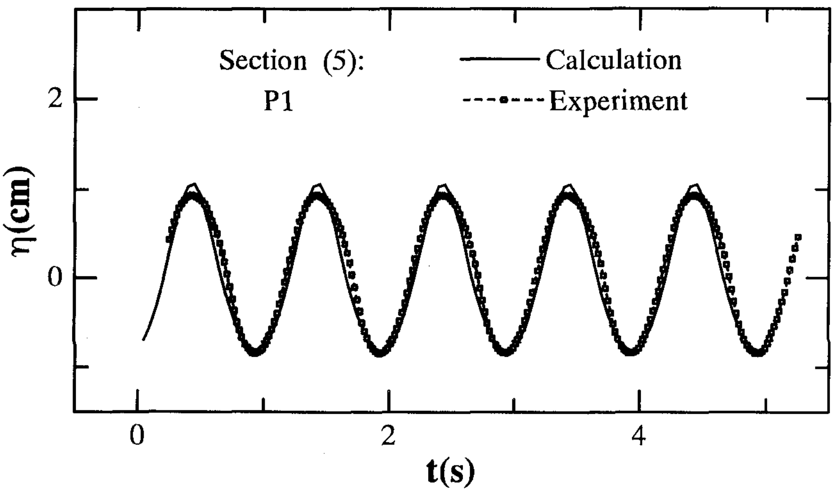

Fig. 4.1 Time history of the surface displacements.

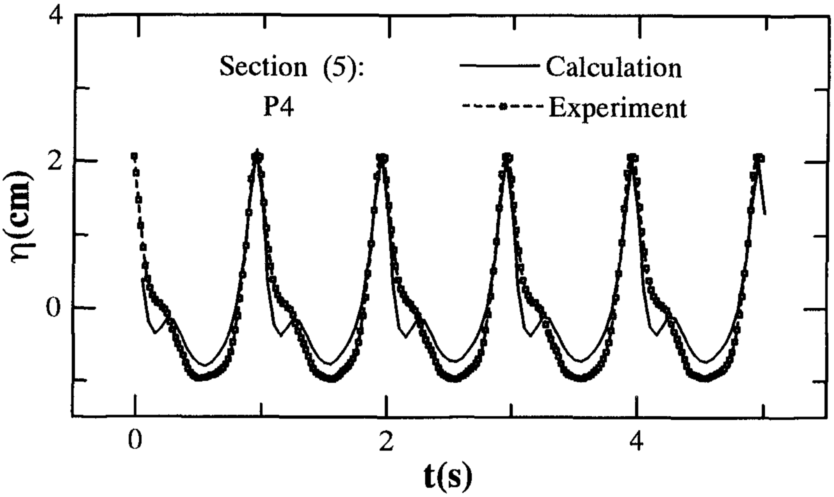

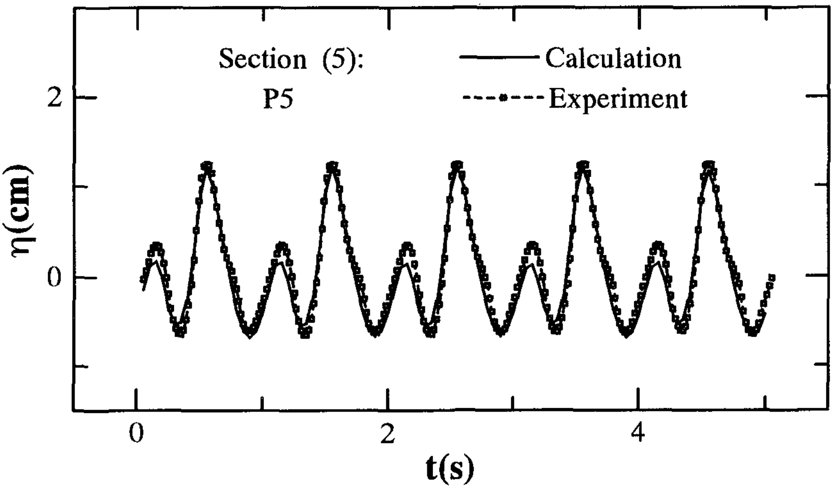

Fig. 4.2 Time history of the surface displacements.

4.2 Conclusions

It has been shown that the agreement between the measurements and the computations is good enough for practical use. For all the other cases, the agreement has been as good as for this case. It will be concluded that the present model reproduces well not only the root mean square wave height distribution but also the temporal variations of surface displacement at every point even when higher harmonic components strongly appear above and behind the breakwater owing to the high nonlinearity of waves.

These results indicate the validity of the present model as well as the interesting effects of the wave direction change due to the presence of a submerged triangular breakwater on the wave deformation.

References

[1] Fletcher, C.A.J. (1987): Computational Techniques for Fluid Dynamics, Vol. I, Springer-Verlag, 252p.

[2] Goda, Y., and Y. Suzuki (1976): Estimation of incident and reflected waves in random wave experiments, Proc. 15th Coastal Eng. Conf., ASCE, pp. 828–845.

[3] Isobe, M. (1994): Time-dependent mild-slope equations for random waves, Proc. 24th Int'l Conf. on Coastal Eng., ASCE, pp. 285–299.